

Lattice Boer-Mulders TMDPDF with LaMET

Lingquan Ma^{a,b,*}

^a*Beijing Normal University, Department of Physics, Beijing Normal University, Beijing 100875, China*

^b*School of Science and Engineering, The Chinese University of Hong Kong, Shenzhen 518172, China*

E-mail: 202031140013@mail.bnu.edu.cn

Transverse-momentum-dependent parton distribution functions (TMDPDFs) are important in revealing the 3D structure of hadrons. Among these distributions, the T-odd Boer-Mulders TMDPDF describes the transversely polarized quark distribution in an unpolarized hadron. Within large-momentum effective theory, we performed a lattice calculation of the nucleon Boer-Mulders function. The calculation was done on the X650 ensemble generated by CLS collaboration with Clover fermion and HYP-smearred gauge links.

The 41st International Symposium on Lattice Field Theory (LATTICE2024)

28 July - 3 August 2024

Liverpool, UK

*Speaker

1. Introduction

The internal structure of nucleons has always been an important topic in both experimental and theoretical explorations. There are many aspects of the explorations, for example, the form factors, the general parton distributions (GPDs), the transverse-momentum-dependent parton distributions (TMDPDFs). TMDPDFs describe the parton distribution of collinear momentum fraction x with transversal momentum k_T , are one of the important parts of so-called nucleon tomograph [1].

At leading-twist accuracy, quark TMDPDFs can be decomposed into eight correlations according to polarizations of nucleon and parton. The Boer-Mulders TMDPDF [2] reflects the distribution of transversely polarized quarks in unpolarized nucleon or pion, which is at the center of our research interests.

There are some investigations on TMDPDFs using lattice calculation [3–5]. However, all these works only calculate the moments of TMDPDFs. Making use of large momentum effective theory (LaMET), the extraction of TMDPDFs becomes direct and practical. The LaMET provides a systematic method to calculate both TMDPDFs and collinear PDFs on lattice. It relates the physical TMDPDFs defined on light cone to equal-time quasi correlations, which can be calculated using lattice QCD [6]. One example of application of LaMET to lattice calculations TMDPDFs, is the nucleon unpolarized TMDPDF in [7].

In our research, we calculate the Boer-Mulders TMDPDF in lattice QCD on ensemble X650 generated by CLS collaboration and adopt the framework of LaMET to analyze our results. We start from the definition of the leading-twist TMDPDF matrix element of the proton on light-cone coordinate system [8],

$$\tilde{\Phi}^0(x, P^+, b_\perp, \mu, \zeta, \Gamma) = \int \frac{db^-}{4\pi} e^{-ib^-(xP^+)} \langle P, S | [\bar{\psi}(b^\mu) \Gamma \mathcal{W}_\square(b_\perp, 0) \psi(0)]_{\mu, \zeta} | P, S \rangle, \quad (1)$$

where the superscript 0 denotes that the matrix element is unrenormalized. $|P, S\rangle$ denotes nucleon with spin S and momentum P along the z -direction, x is the momentum fraction carried by the quark, b_\perp is the Fourier conjugate of parton transverse momentum k_\perp , μ is the renormalization scale in the $\overline{\text{MS}}$ scheme, ζ is the rapidity scale, $\mathcal{W}_\square(b_\perp, 0)$ is the staple-shaped gauge link along the light-cone direction ensuring gauge invariance of the non-local quark bilinear correlator. In the following part of this article, we would omit μ and ζ in Eq. (1). Γ is Dirac matrix inserted in the matrix element,

$$\Gamma \in \{\gamma^+, \gamma^+ \gamma_5, i\sigma^{\alpha+} \gamma_5\}. \quad (2)$$

$\tilde{\Phi}^0$ can be decomposed in eight TMDPDFs. The Boer-Mulders function is one of the terms in the decomposition of the TMDPDF matrix element. We only show the decomposition from which the Boer-Mulders function appears,

$$\tilde{\Phi}^0 = S_T^\alpha \tilde{h}_1 - iS_L b_\perp^\alpha M \tilde{h}_{1L}^\perp + i\epsilon^{\alpha\rho} b_{\perp\rho} M \tilde{h}_1^\perp + \frac{1}{2} b_\perp^2 M^2 \left(\frac{1}{2} g_T^{\alpha\rho} + \frac{b_\perp^\alpha b_\perp^\rho}{b_\perp^2} \right) S_{\perp\rho} \tilde{h}_{1T}^\perp, \quad (3)$$

with $\Gamma = i\sigma^{\alpha+} \gamma_5$. Among the four terms, Boer-Mulders TMDPDF is denoted as \tilde{h}_1^\perp . In the case of unpolarized nucleon external state $S = 0$, only \tilde{h}_1^\perp leaves. This gives a convenience to extract out Boer-Mulders TMDPDF.

On the aspect of lattice QCD, what we need to calculate is an unsubtracted bare quasi-TMD matrix element defined as,

$$\begin{aligned}\tilde{\Phi}^0(z, P, b_\perp, L, a) &= \langle P, S | \hat{O}_\square(z, L, b_\perp) | P, S \rangle, \\ \hat{O}_\square(z, L, b_\perp) &= \bar{\psi}(b^\mu) i\sigma^{\gamma t} \gamma_5 \mathcal{W}_\square(b, L, z) \psi(0),\end{aligned}\quad (4)$$

where the staple-shaped Wilson gauge link \mathcal{W}_\square is lied along z direction and transverse x direction in Euclidean spacetime. \mathcal{W}_\square is defined as

$$\begin{aligned}\mathcal{W}_\square(b_\perp, L, z) &= U_z^\dagger((z+L)\hat{n}_z + b_\perp\hat{n}_\perp, b_\perp\hat{n}_\perp) \times U_\perp((z+L)\hat{n}_z + b_\perp\hat{n}_\perp, (z+L)\hat{n}_z) \\ &\quad \times U_z((z+L)\hat{n}_z, z\hat{n}_z), \\ U_i(\eta + s\hat{n}_i, \eta) &= \mathcal{P}\exp\left[-ig \int_0^s dt \hat{n}_i \cdot A(\eta^\mu + t\hat{n}_i^\mu)\right]\end{aligned}\quad (5)$$

which would take infinite limit $L \rightarrow +\infty$ in renormalization. \hat{n}_z, \hat{n}_\perp are unit vectors along the spatial z and transverse directions, respectively. The unsubtracted bare matrix element (4) contains logarithmic ultraviolet (UV) divergences, linear divergence coming from self-energy corrections to the gauge link [9, 10], as well as the pinch-pole singularity [11, 12], which is related to the heavy quark effective potential term.

After renormalization, we then transform $\tilde{\Phi}^0(z, P, b_\perp, L, a)$ from coordinate space into momentum space quasi-TMD matrix element $\tilde{\Phi}(x, P, b_\perp, \mu, \zeta)$ by

$$\tilde{\Phi}(x, b_\perp, P, \mu, a) = \lim_{L \rightarrow \infty} \int \frac{dz}{2\pi} e^{-iz(xP^z)} \frac{\tilde{\Phi}^0(z, b_\perp, P, L, a)}{\sqrt{Z_E(2L+z, b_\perp, a)} Z_O(a, \mu, \Gamma)}, \quad (6)$$

where $Z_E(r = 2L+z, b_\perp, a)$ is the rectangular Wilson loop with side length equal to b_\perp and $2L+z$. Z_E is obtained by calculating the expectation value of closed rectangular gauge loop. $Z_O(a, \mu, \Gamma)$ is a logarithmic divergence factor depending on some Dirac matrix Γ and used to remove UV divergence and transfer from lattice scheme to $\overline{\text{MS}}$ scheme. Z_O is expressed as

$$Z_O(a, \mu, \Gamma) = \lim_{L \rightarrow \infty} \frac{\tilde{\Phi}^0(z, b_\perp, 0, L, a)}{\sqrt{Z_E(2L+z, b_\perp, a)} \tilde{h}_\Gamma^{\overline{\text{MS}}}(z, b_\perp, \mu)}, \quad (7)$$

the range of z and b_\perp are chosen in a perturbative range. $\tilde{h}_\Gamma^{\overline{\text{MS}}}(z, b_\perp, \mu)$ is a perturbative matrix element of zero momentum up to one-loop order in $\overline{\text{MS}}$ scheme [13]

$$\tilde{h}_\Gamma^{\overline{\text{MS}}}(z, b_\perp, \mu) = 1 + \frac{\alpha_s(\mu) C_F}{2\pi} \left[\frac{1}{2} + \frac{3}{2} \ln\left(\frac{\mu^2(b_\perp^2 + z^2)e^{\gamma_E}}{4}\right) - 2 \frac{z}{b_\perp} \arctan\left(\frac{z}{b_\perp}\right) \right], \quad (8)$$

After renormalization and Fourier transform, we can extract out Boer-Mulders TMDPDF by Eq. (3). The LaMET allows us to related the quasi-TMDPDF \tilde{f} to physical TMDPDF f defined on light cone by a matching formular as,

$$\tilde{f}(x, b_\perp, \zeta_z, \mu) \sqrt{S_I(b_\perp, \mu)} = H_\Gamma\left(\frac{\zeta_z}{\mu^2}\right) e^{\frac{1}{2} \ln\left(\frac{\zeta_z}{\zeta}\right) K(b_\perp, \mu)} f(x, b_\perp, \zeta, \mu) + \mathcal{O}\left(\frac{\Lambda_{\text{QCD}}^2}{\zeta_z}, \frac{M^2}{P_z^2}, \frac{1}{b_\perp^2 \zeta_z}\right), \quad (9)$$

Ensemble	$a(\text{fm})$	$L^3 \times T$	$m_\pi(\text{MeV})$	$m_\pi L$	$N_{\text{conf.}}$
X650	0.098	$48^3 \times 48$	338	8.1	1250

Table 1: The simulation setup, including lattice spacing a , lattice size $L^3 \times T$, the pion masses and the number of configurations.

where S_I denotes the intrinsic soft function [14–16], K is the Collins-Soper kernel [17], μ is the renormalization scale and ζ is the rapidity scale. $\zeta_z = (2xP^z)^2$. The \mathcal{O} term denotes power corrections of the factorization. $H_\Gamma = e^h$ is the hard kernel function at NLO, with

$$h^{(1)} = \frac{\alpha_s C_F}{2\pi} \left(-2 + \frac{\pi^2}{12} + \ln \frac{\zeta}{\mu^2} - \frac{1}{2} \ln^2 \frac{\zeta}{\mu^2} \right). \quad (10)$$

2. Lattice calculation settings

In this project, we use lattice ensemble of X650 generated by the CLS collaboration with lattice spacing $a = 0.098$ fm and pion mass equal to 338 MeV. In order to improve the signal-to-noise ratio of calculations, the following steps have been done: (1) we employ the momentum smearing source technique [18] to improve calculations with high-momentum nucleon states. (2) we apply HYP smearing to further improve the signal. (3) we also use the sequential source method with fixed sink to calculate the quark three-point correlator as illustrated in Fig. 1. (4) we adopt multi-source in our calculation. We put two sources on temporal direction and for spatial shell, we put 2, 2, 1 source(s) respectively on x, y, z axis. We calculate several source-sink separations with hundreds to thousands of measurements among 1250 gauge configurations. Details of the lattice setup and parameters are collected in Table 1.

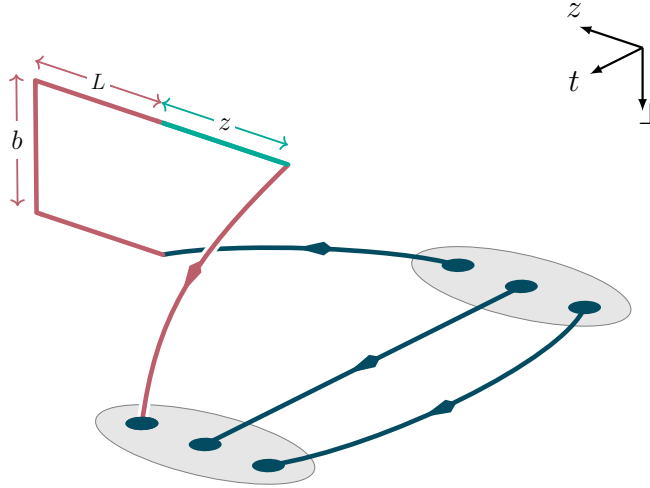


Figure 1: Illustration of three-point function. The temporal direction is from source to sink. S_q denotes quark propagators. The staple-shaped gauge link is put at t . The source-sink separations are set to range from $6a$ to $10a$.

We set the momenta carried by nucleon external state to be $P^z = \{1.32, 1.58, 1.84, 2.11\}$ GeV. We also calculate the zero-momentum bare matrix elements, which are used in the renormalization

factor at short distance. We choose temporal source-sink separations of the following: $t_{\text{sep}} = \{6, 7, 8, 9, 10\}a$. We calculate unsubtracted bare matrix element with b_{\perp} in Eq. (4) up to $3a$. Two-point function $C^{2\text{pt}}(P^z, t_{\text{sep}})$ and three-point function $C^{3\text{pt}}(P^z, t_{\text{sep}}, t)$ are calculated to extract out unsubtracted bare matrix element in Eq. (4):

$$C^{2\text{pt}}(P^z, t_{\text{sep}}) = c_0 e^{-E_0 t_{\text{sep}}} (1 + c_1 e^{-\Delta E t_{\text{sep}}}), \quad (11)$$

$$C^{3\text{pt}}(P^z, t_{\text{sep}}, t) = c_0 e^{-E_0 t_{\text{sep}}} (c_2 + c_3 (e^{-\Delta E t} + e^{-\Delta E (t_{\text{sep}} - t)}) + c_4 e^{-\Delta E t_{\text{sep}}}), \quad (12)$$

where E_0 denotes the ground state energy of nucleon and is dependent on P^z . ΔE is the energy difference between the first excited state and ground state. The staple-shaped gauge link is inserted in time slices t .

3. Lattice results

After calculating two- and three-point functions, the first thing that we check is the dispersion relation of ground state energy $E_0(P^z)$. Considering the discrete effect of lattice, the dispersion relation of ground state is modified to be

$$E_0(P^z) = \sqrt{m^2 + c_1 (P^z)^2 + c_2 (P^z)^4} a^2. \quad (13)$$

which should return to the continuous dispersion relation as lattice spacing $a \rightarrow 0$. By fitting two-point function data of various momenta using Eq. (11) we get ground state energies, and by Eq. (13) we can check whether discrete dispersion relation is satisfied.

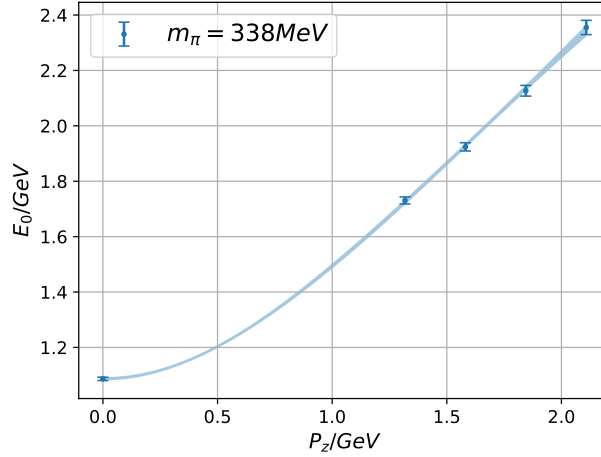


Figure 2: Illustration of the discrete dispersion relation of all P^z 's. This fitting works well even for largest P^z . The fitted nucleon mass is 1.087(6) GeV. The fitted parameters $c_1 = 1.073(40)$, and $c_2 = -0.094(50)$.

We plot the dispersion relations in FIG. 2. It shows that the discrete dispersion relation is satisfied well. And the fitted results of dimensionless parameters c_1 and c_2 are consistent with our expectation that $c_1 \approx 1$, $c_2 \approx 0$. The static mass of nucleon is 1.087(6) GeV. The fitted parameters $c_1 = 1.073(40)$, and $c_2 = -0.094(50)$.

We then adopt joint fitting of two-point function and ratio of $3pt/2pt$ to get parameters $c_0 \sim c_4$ as well as E_0 and ΔE in Eq. (11) and Eq. (12). We denote ratio of $3pt/2pt$ as $R(P^z, t, t_{sep})$,

$$R(P^z, t, t_{sep}) = \frac{C^{3pt}(P^z, t_{sep}, t)}{C^{2pt}(P^z, t_{sep})} = \frac{c_2 + c_3(e^{-\Delta Et} + e^{-\Delta E(t_{sep}-t)}) + c_4 e^{-\Delta Et_{sep}}}{1 + c_1 e^{-\Delta Et_{sep}}} \quad (14)$$

where it can be checked that the parameter $c_2 = \langle P, S | \hat{O}_\square(z, L, b_\perp) | P, S \rangle / 2E_0(P_z)$. c_2 is dependent on (z, L, b_\perp) . Bootstrap resampling is applied in our analysis to obtain correlations in the dataset before joint fitting. We exclude the points at $t = 0$ and $t = t_{sep}$ in order to reduce the contamination effects from excited states. Considering the bad signal-to-noise ratio of larger t_{sep} , for $P^z = \{0, 1.32, 1.58\}$ GeV we use $t_{sep} = \{6, 7, 8, 9\}a$; for $P^z = \{1.84, 2.11\}$ GeV we use $t_{sep} = \{6, 7, 8\}a$.

We use the Wilson loop and logarithmic factor Z_O in the integrated part of Eq. (6) to fulfill the renormalization. After that, we get the subtracted quasi-TMDPDF matrix element denoted as $\tilde{\Phi}(z, b_\perp, P^z, L, a)$. For fixed (z, b_\perp, P^z) , we observe a convergence tendency with L varying. Considering the signal-to-noise ratio decreases with L increasing, we find that the convergence shows itself the best in the interval $[6, 10]a$. In Fig. 3, we take $P^z = 1.32$ GeV and 1.84 GeV and $b_\perp = 1a$ and $2a$ as example to show the convergence trend of large L . The convergence indicates the existence of infinite L limit of $\tilde{\Phi}(z, b_\perp, P^z, L, a)$.

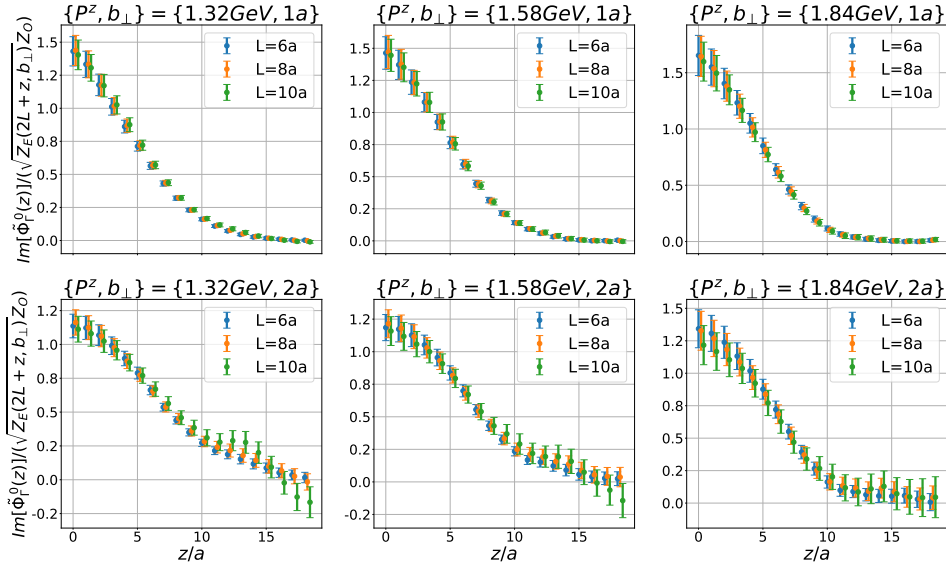


Figure 3: Illustration of the subtracted quasi-TMDPDF $\tilde{\Phi}(z, b_\perp, P^z, L, a)$. The upper panel is plotted for $P^z = 1.32$ GeV, 1.58 GeV, 1.84 GeV with $b_\perp = 1a, 2a$; the lower panel is for $P^z = 1.84$ GeV with $b_\perp = 1a, 2a$. The convergence with L increasing has shown in the plots, which indicates existence of infinite limit of L .

For L larger than $10a$, the errors become so large that all L data is consistent in one sigma. In practice, regarding both the convergence and magnitude of error, we consider to use data of $L = 8a$ as an estimate of infinite L . We then step to the Fourier transform by Eq. (6). Before doing Fourier transform, we use extrapolated values instead of original $\tilde{\Phi}(z, b_\perp, P^z, L, a)$ in the range of large

$\lambda = zP^z$. By this replacement we try to get rid of unphysical oscillations in quasi-TMDPDFs. The extrapolation is done by the form as [19],

$$\tilde{\Phi}_{\text{extra}}(\lambda) = \left[\frac{m_1}{(-i\lambda)^{n_1}} + e^{i\lambda} \frac{m_2}{(i\lambda)^{n_2}} \right] e^{-\lambda/\lambda_0}, \quad (15)$$

where parameters $m_{1,2}$, $n_{1,2}$ and λ_0 are by default dependent on b_\perp . We fit separately each b_\perp making use of Eq. (15). After that we Fourier transform $\Phi(z, b_\perp, P^z, L = 8a, a)$ from coordinate space to momentum space by Eq. (6). We get the quasi-Boer-Mulders TMDPDF $\tilde{h}_1^\perp(x, b_\perp, P^z, a)$ according to the decomposition shown in Eq. (3).

The matching of quasi-TMDPDF $\tilde{h}_1^\perp(x, b_\perp, P^z, a)$ to physical TMDPDF $h_1^\perp(x, b_\perp, P^z, a)$ done by Eq. (9) use lattice calculated intrinsic soft function S_I and Collins-Soper kernel $K(b_\perp, \mu)$ on ensemble X650 [20]. The method of error-propagation is used to obtain error of $h_1^\perp(x, b_\perp, P^z, a)$. In FIG. 4, we show preliminary results of $h_1^\perp(x, b_\perp, P^z, a)$ for $b = 1 \sim 3a$, with all momenta plotted together. We see a convergent trend of various P^z , which gives a trend that large momentum extrapolation can be implemented to get rid of momentum dependence and get a final Boer-Mulders TMDPDF defined on light cone. Note that the results at small x is unreliable with exploring errors. For fixed x , it shows a decaying trend with b_\perp getting larger. This suggests that the Boer-Mulders function might receive smaller higher-twist contributions.

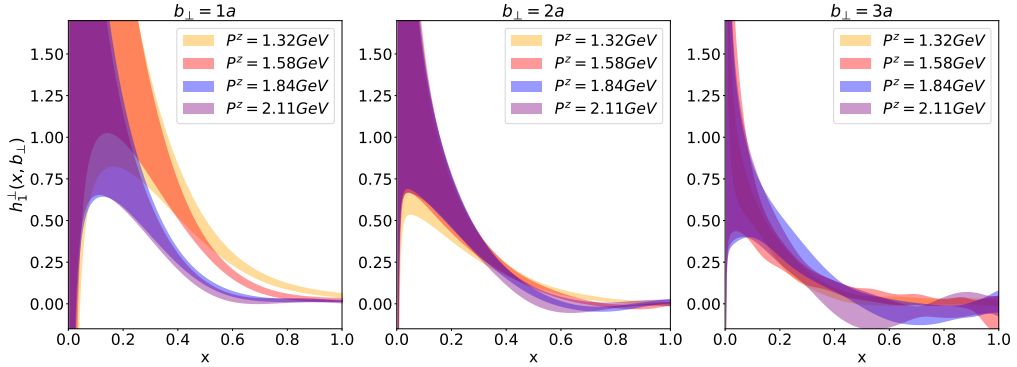


Figure 4: Illustration of the subtracted physical Boer-Mulders TMDPDF $h_1^\perp(z, b_\perp, P^z, L, a)$ for $b_\perp = 1a, 2a, 3a$. With P^z getting larger, $h_1^\perp(x, b_\perp, P^z, a)$ is getting convergent.

4. Summary

In this proceeding, we introduce the theoretical framework of lattice calculation on TMDPDF, the LaMET is used as the tool to extract physically defined Boer-Mulders TMDPDF. We show the settings of lattice calculations on the momenta and source-sink separations and how we improve the signal-to-noise ratio. Combined fit of two- and three-point function to obtain the quasi-matrix elements is used. We do the renormalization and show the convergence of large L . Fourier transformation and matching are done to get physical TMDPDF.

We will do a more detailed analysis to get more accurate results. We will apply resummation method using NNLO results of Eq. (8) and Eq. (10). Finally, we will do large momentum extrapolation by fitting and analyze the b_\perp dependence of $h_1^\perp(x, b_\perp, P^z, a)$.

Acknowledgments

This work was supported by the High Performance Computing Center of Central South University. We thank the CLS Collaboration for sharing the lattices used to perform this study. The LQCD calculations were performed using the multigrid algorithm [21, 22] and Chroma software suite [23]. This work is supported by the National Natural Science Foundation of China under grants No. 12375080, 11975051, and by CUHK-Shenzhen under grant No. UDF01002851.

References

- [1] N. G. Stefanis, C. Alexandrou, T. Horn, H. Moutarde and I. Scimemi, *Round table: Nucleon tomography. What can we do better today than Rutherford 100 years ago?*, *EPJ Web Conf.* **137** (2017) 01003 [1612.03077].
- [2] D. Boer and P. J. Mulders, *Time reversal odd distribution functions in leptonproduction*, *Phys. Rev. D* **57** (1998) 5780 [9711485].
- [3] M. Engelhardt, P. Hägler, B. Musch, J. Negele and A. Schäfer, *Lattice QCD study of the Boer-Mulders effect in a pion*, *Phys. Rev. D* **93** (2016) 054501 [1506.07826].
- [4] B. Yoon, M. Engelhardt, R. Gupta, T. Bhattacharya, J. R. Green, B. U. Musch, J. W. Negele, A. V. Pochinsky, A. Schäfer and S. N. Syritsyn, *Nucleon Transverse Momentum-dependent Parton Distributions in Lattice QCD: Renormalization Patterns and Discretization Effects*, *Phys. Rev. D* **96** (2017) 094508 [1706.03406].
- [5] C. Alexandrou, S. Bacchio, M. Constantinou, P. Dimopoulos, J. Finkenrath, R. Frezzotti, K. Hadjiyiannakou, K. Jansen, B. Kostrzewa and G. Koutsou, *Moments of the nucleon transverse quark spin densities using lattice QCD*, *Phys. Rev. D* **107** (2023) 054504 [2202.09871].
- [6] X. Ji, *Parton Physics on a Euclidean Lattice*, *Phys. Rev. D* **110** (2013) 262002 [1305.1539].
- [7] J. C. He *et al.* [Lattice Parton Collaboration (LPC)], *Unpolarized transverse momentum dependent parton distributions of the nucleon from lattice QCD*, *Phys. Rev. D* **109** (2024) 114513 [2211.02340].
- [8] R. Boussarie, M. Burkardt, M. Constantinou, W. Detmold, M. Ebert, M. Engelhardt, S. Fleming, L. Gamberg, X. Ji and Z. B. Kang, *et al.*, *TMD Handbook* 2304.03302.
- [9] P. Shanahan, M. L. Wagman and Y. Zhao, *Nonperturbative renormalization of staple-shaped Wilson line operators in lattice QCD*, *Phys. Rev. D* **101** (2020) 074505 [1911.00800].
- [10] Y. Ji, J. H. Zhang, S. Zhao and R. Zhu, *Renormalization and mixing of staple-shaped Wilson line operators on the lattice revisited*, *Phys. Rev. D* **104** (2021) 094510 [2104.13345].
- [11] X. Ji, J. H. Zhang and Y. Zhao, *Renormalization in Large Momentum Effective Theory of Parton Physics*, *Phys. Rev. Lett.* **120** (2018) 112001 [1706.08962].

- [12] X. Ji, Y. Liu, A. Schäfer, W. Wang, Y. B. Yang, J. H. Zhang and Y. Zhao, *A Hybrid Renormalization Scheme for Quasi Light-Front Correlations in Large-Momentum Effective Theory*, *Nucl. Phys. B* **964** (2021) 115311 [2008.03886].
- [13] K. Zhang *et al.* [Lattice Parton (LPC)], *Renormalization of Transverse-Momentum-Dependent Parton Distribution on the Lattice*, *Phys. Rev. Lett.* **129** (2022) 082002 [2205.13402].
- [14] X. Ji, Y. Liu and Y. S. Liu, *TMD soft function from large-momentum effective theory*, *Nucl. Phys. B* **955** (2020) 115054 [1910.11415].
- [15] Q. A. Zhang *et al.* [Lattice Parton], *Lattice-QCD Calculations of TMD Soft Function Through Large-Momentum Effective Theory*, *Phys. Rev. Lett.* **125** (2020) 192001 [2005.14572].
- [16] Y. Li, S. C. Xia, C. Alexandrou, K. Cichy, M. Constantinou, X. Feng, K. Hadjiyiannakou, K. Jansen, C. Liu and A. Scapellato, *et al.* *Lattice QCD Study of Transverse-Momentum Dependent Soft Function*, *Phys. Rev. Lett.* **128** (2022) 062002 [2106.13027].
- [17] M. H. Chu *et al.* [Lattice Parton (LPC)], *Nonperturbative determination of the Collins-Soper kernel from quasitransverse-momentum-dependent wave functions*, *Phys. Rev. D* **106** (2022) 034509 [2204.00200].
- [18] G. S. Bali, B. Lang, B. U. Musch and A. Schäfer, *Novel quark smearing for hadrons with high momenta in lattice QCD*, *Phys. Rev. D* **93** (2016) 094515 [1602.05525].
- [19] Xiangdong Ji, Yizhuang Liu, Andreas Schäfer, Wei Wang, Yi-Bo Yang, Jian-Hui Zhang, Yong Zhao, *A hybrid renormalization scheme for quasi light-front correlations in large-momentum effective theory*, *Nucl. Phys. B* **964** (2021) 115311 [2008.03886].
- [20] M. H. Chu *et al.* [Lattice Parton (LPC)], *Lattice calculation of the intrinsic soft function and the Collins-Soper kernel*, *JHEP* **08** (2023) 172 [2306.06488].
- [21] R. Babich, J. Brannick, R. C. Brower, M. A. Clark, T. A. Manteuffel, S. F. McCormick, J. C. Osborn and C. Rebbi, *Adaptive multigrid algorithm for the lattice Wilson-Dirac operator*, *Phys. Rev. Lett.* **105** (2010) 201602 [1005.3043].
- [22] J. C. Osborn, R. Babich, J. Brannick, R. C. Brower, M. A. Clark, S. D. Cohen and C. Rebbi, *Multigrid solver for clover fermions*, *PoS LATTICE2010* (2010) 037 [1011.2775].
- [23] R. G. Edwards *et al.* [SciDAC, LHPC and UKQCD], *The Chroma software system for lattice QCD*, *Nucl. Phys. B Proc. Suppl.* **140** (2005) 832 [0409003].